Effects of fluctuating daily surface fluxes on the time-mean oceanic circulation

Effects of fluctuating daily surface fluxes on the time-mean oceanic circulation

[†]Balan Sarojini Beena and Jin-Song von Storch

Max-Planck Institute for Meteorology, Hamburg, Germany

March 28, 2009

revised version to *Climate Dynamics*

Corresponding author: Jin-Song von Storch
Max-Planck Institute for Meteorology
Bundestrasse 53, 20146 Hamburg, Germany
Phone: +49 40 41173 155, Fax: +49 40 41173 366
Email: jin-song.von.storch@zmaw.de

[†]Present address: National Centre for Atmospheric Science - Climate,
Walker Institute for Climate System Research, Department of Meteorology
University of Reading, Reading RG6 6BB, United Kingdom

Abstract

The effect of fluctuating daily surface fluxes on the time-mean oceanic circulation is studied using an empirical flux model. The model produces fluctuating fluxes resulting from atmospheric variability and includes oceanic feedbacks on the fluxes. Numerical experiments were carried out by driving an ocean general circulation model with three different versions of the empirical model. It is found that fluctuating daily fluxes lead to an increase in the Meridional Overturning Circulation (MOC) of the Atlantic of about 1 Sv and a decrease in the Antarctic Circumpolar Current (ACC) of about 32 Sv. The changes are approximately 7% of the MOC and 16% of the ACC obtained without fluctuating daily fluxes.

The fluctuating fluxes change the intensity and the depth of vertical mixing. This, in turn, changes the density field and thus the circulation. Fluctuating buoyancy fluxes change the vertical mixing in a non-linear way: They tend to increase the convective mixing in mostly stable regions and to decrease the convective mixing in mostly unstable regions. The ACC changes are related to the enhanced mixing in the subtropical and the mid-latitude Southern Ocean and reduced mixing in the high-latitude Southern Ocean. The enhanced mixing is related to an increase in the frequency and the depth of convective events. As these events bring more dense water downward, the mixing changes lead to a reduction in meridional gradient of the depth-integrated density in the Southern Ocean and hence the strength of the ACC. The MOC changes are related to more subtle density changes. It is found that the vertical mixing in a latitudinal strip in the northern North Atlantic is more strongly enhanced due to fluctuating fluxes than the mixing in a latitudinal strip in the South Atlantic.

This leads to an increase in the density difference between the two strips, which can be responsible for the increase in the Atlantic MOC.

Keywords : Fluctuating daily fluxes, Vertical mixing, Meridional Overturning Circulation, Antarctic Circumpolar Current, Air-Sea interaction.

1 Introduction

The issue of what determines the strength of the global Meridional Overturning Circulation (MOC) has drawn the attention of many researchers. The prevailing view is that the circulation is driven partly by the diapycnal mixing of heat that lightens water masses in the deep ocean and causes them to rise uniformly in low latitudes (Munk and Wunsch 1998), and partly by wind-driven upwelling induced by the strong westerly circumpolar winds in the Southern Ocean (Webb and Suginohara 2001, Toggweiler and Samuels 1995). Both the diapycnal mixing and the wind-driven upwelling focus on the mechanisms that allow deep dense water masses to return to the surface. The surface buoyancy forcing, though not considered as a driver of the MOC capable for providing energy supply, is necessary for setting up the flow by controlling the rate and site of the deep water formation (Kuhlbrodt et al. 2007).

The major factors which control the MOC in the above picture are the diapycnal mixing, the upwelling due to wind forcing and the rate and the site of deep water formation set up by the surface buoyancy forcing. All these factors are directly or indirectly related to the air-sea fluxes. So far, the analyses have mainly focused on the effects of *climatological mean* components of the wind forcing in providing the energy required for diapycnal mixing or in inducing wind-driven upwelling (Munk and Wunsch 1998, Webb and Suginohara 2001, Toggweiler and Samuels 1995). This paper aims at a detailed picture that can isolate the effect of *fluctuating day-to-day fluxes* from that of the mean fluxes.

Generally, the role of air-sea fluxes in determining the stratification and the circulation of the oceans has been known for long time. Such a role has been investigated within theoretical frameworks (Walin 1982 and Tziperman 1986) and with respect to change in convection (Rahmstorf 1995, Kuhlbrodt and Monahan 2003, Swingedouw et al. 2007). Walin (1982) studied the relation between sea-surface heat flux and thermal circulation in the ocean. Tziperman (1986) derived a relation between the interior stratification and the air-sea heat fluxes and used this relation to study the buoyancy driven circulation. The role of surface flux anomalies in triggering convection was studied by Rahmstorf (1995). Using a simple box model, Kuhlbrodt and Monahan (2003) showed that the variability of surface fluxes is important for the open ocean convection and deep water formation in the Labrador Sea. Swingedouw et al. (2007) found a linear relationship between density changes in the convection sites and the strength of the Atlantic MOC.

Even though the previous studies support the important role of day-to-day anomalies of air-sea fluxes, it is generally difficult to obtain a quantitative estimation of the impact of all fluctuating fluxes on the MOC in the framework of GCMs. For instance, it is obvious that an evaporation anomaly can lead to the formation of water denser than 1028 kg/m^3, while a precipitation anomaly can lead to the formation of water lighter than 1028 kg/m^3. With these anomalies, water mass production denser than 1028 kg/m^3 can occur. Without these anomalies, but with the same time-mean buoyancy forcing, the water mass production denser than 1028 kg/m^3 would have been zero. However, what is less clear is the net effect of all buoyancy anomalies on the oceanic circulation.

The effect of fluctuating fluxes can be strongly non-linear. For example, consider buoyancy anomalies occuring in a mostly stable region. In this case, positive anomalies (e.g. due to a precipitation event or a downward positive heat flux anomaly) may not significantly affect the statistics of convective events (since the water column is already stable), whereas negative anomalies (e.g. due to an evaporation event or a negative heat flux anomaly) could significantly increase convective events, resulting in non-linear responses to fluctuating fluxes.

Given the potential and complexity of daily air-sea fluxes in changing the water mass production and from that the interior stratification and circulation, the effect of daily fluxes is investigated using a coupled system, specially developed for this purpose. The system consists of an ocean GCM and an empirical global flux model which describes the day-to-day flux variations in a realistic manner. The advantage of this system is that it allows a separation of effects of fluctuating air-sea fluxes from that of the climatological mean fluxes. Such a separation is difficult within a fully coupled atmosphere and ocean GCM. Numerical experiments were carried out using the hybrid coupled model. As will be shown, the fluctuating daily fluxes affect not only the Atlantic MOC, but also the Antarctic Circumpolar Current (ACC). The models and the numerical experiments are described in Section 2 and 3. The results of the experiments are presented in Section 4. Discussion and conclusions are given in the final section.

2 Model Description

The empirical flux model and the OGCM used in this study are briefly introduced below. A more detailed description can be found in von Storch et al. (2005) and Marsland et al. (2003).

2.1 The empirical model of daily air-sea fluxes: EMAD

The flux model, referred to as EMAD (Empirical Model of Atmospheric Dynamics), is designed to generate air-sea flux anomalies relative to given climatological mean fluxes. Based on the assumption that deviations from a given mean state of the coupled system are small, the dynamics of the flux anomalies and the response of these fluxes to anomalous sea surface condition are considered to be linear and described by

$$\mathbf{x}'_{t+1} = \mathcal{A}\mathbf{x}'_t + \mathcal{C}\mathbf{n}_{t+1} + \mathcal{B}\mathbf{y}'_t. \tag{1}$$

$\mathbf{x}'$ comprises anomalies of all fluxes required to drive the OGCM. These are the net heat flux, the zonal and meridional momentum flux, the freshwater flux, the short-wave radiation which penetrates into the sea water, and the conductive and residual heat flux required to describe the sea ice formation and depletion. $\mathbf{y}'$ represents anomalies of oceanic variables at the sea surface, such as the SST, the sea ice cover and the sea ice thickness, that can affect the fluxes. $\mathbf{n}$ is a multivariate white noise with zero mean and unit variance. $\mathcal{A}$ describes the linear dynamics of the fluxes, $\mathcal{B}$ the linear response of fluxes to the ocean surface condition, and $\mathcal{C}$ the covariance structure of the residual that is not depicted by $\mathcal{A}$ and $\mathcal{B}$. The time step of Eq.(1)

is one day.

$\mathcal{A}$, $\mathcal{B}$ and $\mathcal{C}$ are matrices obtained by fitting Eq.(1) on to the daily output of a 200-year control integration performed with the fully coupled ECHO-G Atmosphere Ocean General Circulation Model (AOGCM) (Legutke and Voss 1999 ; Raible et al. 2001). The fitting is done first for $\mathcal{A}$ and $\mathcal{B}$ in EOF-spaces represented by the leading EOFs of fluxes and then for $\mathcal{C}$ in the physical space. We use 100 EOFs for each flux and 100 EOFs for SST in the water module (further explained below) and 50 EOFs for each of the same variables in the ice module. The physical space has the Gaussian grid of T30 resolution.

The EMAD model consists of a water module and an ice module for the separate treatment of the fluxes over permanently open water and sea surface where ice can be formed. The formulation of the two modules is necessary to deal with the additional fluxes which are required to drive the sea-ice model. Different from the water module, the state vector $\mathbf{x}'$ in the ice module contains the conductive and residual heat and distinguishes the fluxes of net heat, fresh water and momentum over ice and water. Depending on the sea ice fraction within a grid cell, either the fluxes over ice or the fluxes over water or both will be used to drive the ocean.

Without the last term, the model equation (1) mimics the linear dynamics of flux anomalies driven by the atmospheric variability. The last term with $\mathcal{B}$ describes the oceanic feedbacks on the fluxes. Since $\mathcal{B}$ is derived from a coupled model integration which is essentially statistically stationary, the interaction described by $\mathcal{B}\mathbf{y}'$ acts to keep the ocean in the given mean state. This means that, if the sea surface condition is moved away from the given sea surface state, there would be non-zero anomalies of sea surface variables and from that a non-zero $\mathbf{y}'$, which generates anomalous fluxes $\mathcal{B}\mathbf{y}'$ that drive the sea surface back to the given state.

The just described feedback mechanism involves essentially the interaction between the heat flux and the SST anomalies. It functions in a way as if the heat flux is described by a restoring condition. However, in contrast to the traditional restoring formulation which uses a constant restoration time, $\mathcal{B}$ implies a dependence of the restoration time on spatial scales. By formulating in EOF-space, $\mathcal{B}$ captures the restoring time scales for modes with different spatial scales in the ECHO-G integration. In particular, large-scale SST anomalies are allowed to exist over a longer time period, while small-scale SST anomalies will be damped out quickly. The need for such a scale-dependent restoration was first pointed out by Rahmstorf and Willebrand (1995). The present formulation can be considered as an empirical approach that captures the scale-dependent feedback of SST on heat flux in the ECHO-G integration. Due to the scale dependence, the $\mathcal{B}\mathbf{y}'$-term does not act as a rigid restoring. One does not obtain exactly the same SST when using $\mathcal{B}\mathbf{y}'$ to nudge SSTs to the same climatological mean SST (see Section 4.1).

By collecting all fluxes into vector $\mathbf{x}'$ and all relevant sea surface variables in vector $\mathbf{y}'$, the model equation (1) ensures that the fluxes and the oceanic variables are physically coherent. When coupling EMAD to an OGCM, the fluxes of heat, fresh water and momentum will not respond independently to a given anomalous state of the sea surface.

The noise term acts to excite the EOF-modes described by the deterministic part of EMAD (i.e. by $\mathcal{A}$- and $\mathcal{B}$-terms). The matrix $\mathcal{C}$ ensures that the distributions of the total variances of the fluxes match those obtained from the coupled ECHO-G model.

Despite the extremely simple form, the model equation (1) is able to describe various types of air-sea interactions. If $\mathcal{A}\mathbf{x}^{'} + \mathcal{C}\mathbf{n}$ dominates $\mathcal{B}\mathbf{y}^{'}$ for a certain flux, this flux would force the ocean by and large stochastically. This could be the case for wind stress anomalies over high-latitudes, where the influence of the SST on the wind stress is weak. If the $\mathcal{A}$-term and the $\mathcal{B}$-term have similar strength, the flux would be affected both by the stochastic forcing and by the oceanic feedback. If the $\mathcal{B}$-term dominates, the flux would be essentially determined by the oceanic conditions. The relative importance of the various types of air-sea interactions is given by the amplitudes of elements of $\mathcal{A}$ and $\mathcal{B}$. The result of different types of air-sea interactions can be identified by studying the lagged correlation functions between the flux and SST (Frankignoul et al. 1998 ; von Storch 2000).

The ability of EMAD in reproducing the second moments of fluxes found in the coupled ECHO-G is considered in von Storch et al. (2005). In particular, it was shown that EMAD produces variances of fluxes, whose strength and distribution are in general comparable to that found in ECHO-G. The various types of interactions, as can be identified using the lagged correlation functions between the SST and the fluxes (Frankignoul et al. 1998 ; von Storch 2000), are by and large reproduced when coupling EMAD to an OGCM. Finally, EMAD is able to act realistically to anomalous sea surface condition, such as those related to an ENSO event or to a Polynya.

To give the reader an idea of how the EMAD-fluxes look like, Figure 1 shows anomalies of wind stress (arrows) and heat flux (colour shading), obtained by forcing EMAD with the anomalous sea surface conditions derived from the coupled ECHAM5/MPI-OM AOGCM (Jungclaus et al. 2005). Also shown in Figure 1 is a snapshot of the anomalies of the same fluxes from the NCEP reanalysis for an arbitrary day. Similar to the fluxes of the reanalysis, the EMAD-fluxes have maxima at the mid- and high-latitudes. The amplitudes of EMAD-anomalies are slightly larger than those of the reanalysis. The structure of the EMAD-anomalies are somewhat smoother than that of the NCEP-fluxes, reflecting the fact that EMAD describes the leading EOF-modes excited by white noise forcing. Figure 1 and the previous validation (von Storch et al. 2005) suggest that EMAD is capable of producing the basic features of the fluctuating day-to-day fluxes.

2.2 The Ocean General Circulation Model: MPI-OM

The OGCM used in this study is the Max-Planck Institute Ocean Model (MPI-OM). It is a z-coordinate model based on primitive equations for a Boussinesq fluid on a rotating sphere. It is formulated on the horizontal Arakawa C grid with the north pole located at northern Greenland and south pole close to Weddell Sea. It has horizontal resolution varying from 20 km in the main sinking regions associated with the MOC to about 350 km in the tropics. For the present study, the model configuration with 40 vertical levels (Haak et al. 2003) is used. The model contains a free surface and a state-of-the-art sea ice model with viscous-plastic rheology and snow. Overflow over the sills and off continental shelves are represented by a bottom boundary layer slope convection scheme.

Tracer diffusion is isoneutral and dianeutral and is described by the diffusion tensor $\mathcal{K}$ (Redi 1982), which is a function of the neutral density gradient and horizontal and vertical diffusion coefficients K_H and K_V. The scheme is numerically implemented following Griffies (1998). The effect of horizontal tracer mixing by advection due to the unresolved mesoscale eddies is parameterized after Gent et al. (1995). The horizontal eddy viscosity is parameterized using a scale-dependent biharmonic formulation. The vertical eddy viscosity follows Pacanowski and Philander (1981). It utilizes an eddy coefficient which is represented in the same way as the vertical eddy diffusivity coefficient K_V (see Eq.(2) below), except that the Richardson-number dependent part is proportional to $(1 + C_{RD}R_i)^{-2}$, rather than $(1 + C_{RD}R_i)^{-3}$ as given in Eq.(3). The vertical diffusion, as described by K_V or in short K, plays an important role in the present study and is further described below.

K is a function of convective mixing, Richardson number (Ri) dependent mixing, wind-induced mixing and background diffusivity (Marsland et al. 2003) and is given by

$$K = \begin{cases} K_{conv} & \text{if statically unstable} \\ K_{Ri} + K_{wind} + K_{back} & \text{if statically stable} \end{cases} \tag{2}$$

with

$$K_{Ri} = D_{VO}(1 + C_{RD}R_i)^{-3}, \tag{3}$$

where R_i is the Richardson number, $D_{VO} = 2 \times 10^{-3}$ m^2s^{-1} and $C_{RD} = 5$ are model constants. According to Eq.(3), the maximum value of K_{Ri} is 2×10^{-3} m^2s^{-1}. The diffusion related to convection K_{conv} is set to 10^{-1} m^2/s. Thus, static instability is removed by switching on an extremely strong mixing. In the surface layer, the wind-induced mixing K_{wind} over ice free regions is given by

$$K_{wind} = W_T V_{10}^3 \tag{4}$$

where V_{10} is the local 10 m wind speed and W_T equals 5×10^{-4} $m^{-1}s^2$. Below the surface, K_{wind} depends on the stability of the water column and decays exponentially with e-folding depth being 40 m. The diffusion related to other unresolved processes, such as internal waves, is described by $K_{back} = 10^{-5}$ m^2/s. This set of parameters is used in the integration of MPI-OM coupled to the ECHAM5 AGCM (Jungclaus et al. 2005) that produces a realistic oceanic state.

The vertical diffusion coefficient K can vary spatially and temporally, depending on the static stability and wind forcing. Since K_{back} is unchanged in the experiments performed and since K_{wind} is confined to the first 40 meters of the ocean (depending on the stability), the changes in K below 40 meters are related to the changes in K_{Ri} and / or K_{conv}. Fluctuating fluxes can change both K_{Ri} and K_{conv}.

Fluctuating fluxes can affect K_{conv} by turning convection on and off in a non-linear way, depending on the background static stability. In the regions where the stratification is mostly stable and K_{conv} is mostly turned off, a positive buoyancy forcing (induced e.g. by additional precipitation events or additional heat flux anomalies) makes the ocean more stable and hence will leave K_{conv} switched off. By contrast, a negative buoyancy forcing will reduce static stability, and hence K_{conv} might be switched on more often. The net effect is an increase in the convective mixing. Examples of mostly stable oceans are the tropical and subtropical oceans. On the other hand, in regions where the stratification is mostly unstable and K_{conv} is mostly switched on, a negative buoyancy forcing will not affect the convective mixing much, since the convective mixing is already switched on. A positive buoyancy anomaly on the contrary can increase the static stability, making K_{conv} switched on less often. The net effect is a decrease in K. Examples of mostly unstable oceans are the GIN (Greenland Iceland Norwegian) Seas and the high-latitude Southern Ocean in the MPI-OM model.

The above described changes in convective events are not inconsistent with previous numerical experiments in which the convection at single grid points can be switched on and off by flux anomalies and be crucial for maintaining deep water formation (Rahmstorf 1995, Kuhlbrodt and Monahan 2003).

Fluctuating fluxes can also change the Ri-dependent mixing, since a fluctuating buoyancy flux can affect the stratification of the water column and a fluctuating wind stress forcing can alter the shear of the current. The change in the Ri-dependent mixing is expected to be more pronounced in the tropics. In these regions, the static stability of the ocean is so high that static instability rarely occurs and, when it occurs, it will be confined to a shallow surface layer.

In the present study, the vertical diffusion coefficient K is stored on monthly basis. Since the maximum value of K_{Ri} of 2×10^{-3} $m^2 s^{-1}$ is much smaller than $K_{conv} = 10^{-1}$ m^2/s, large changes in K must be related to changes in the number of convective events occurring within a month. Generally, a large increase (decrease) in K indicates an increase (a decrease) in the number of convective events, and from that an increase (a decrease) in the formation of dense water masses. In this sense, changes in K can be used as a crude measure of changes in water mass formation due to convection. As shown by the mean convection depth in Figure 10a, the true deep water formation, reaching about 1000 meter depth on average, occurs only in GIN seas and off the Antarctic coast in the Atlantic sector in the version of the MPI-OM model used here.

2.3 The Coupled Model: EMAD/MPI-OM

To couple the EMAD with the MPI-OM, the EMAD fluxes, which are on the T30-Gaussian grid, are interpolated into the curvilinear grid of the MPI-OM model. The coupling takes place once a day.

When coupling EMAD to the MPI-OM model, one needs a set of fields of climatological mean fluxes and a set of fields of climatological mean sea surface conditions. Both sets were derived from the last 50 years of a 600-year integration with the ECHAM5/MPI-OM coupled AOGCM (Jungclaus et al. 2005). The climatology contains the annual cycle on a daily basis. Given an oceanic state at time t, the anomalous sea surface condition $\mathbf{y}^{'}$ is derived by subtracting the actual oceanic state from the given climatological mean state. With this $\mathbf{y}^{'}$ and the anomalous flux forcing $\mathbf{x}^{'}$ at $t-1$, EMAD produces the anomalous flux forcing at t. Adding this to the climatological mean forcing gives the net flux forcing at time t which is used to produce $\mathbf{y}^{'}$ at time $t+1$.

It should be noted that since EMAD is only an approximation of ECHAM5, and since the $\mathcal{B}\mathbf{y}'$-term is not a rigid restoring, the climatological mean state produced by the MPI-OM model coupled to EMAD generally does not match the climatological mean state produced by the fully coupled ECHAM5/MPI-OM. As a consequence, the time-mean of $\mathbf{y}^{'}$ is not zero. This non-zero time-mean of $\mathbf{y}^{'}$ can feed back to the fluxes and produce non-zero time-mean of $\mathbf{x}^{'}$, whereby complicating the interpretation of the experiments to be introduced in Section 3. We will return to this issue later.

Apart from the feedbacks described by $\mathcal{B}$, there is no relaxation of salinity or temperature in the ocean. The only procedure used to prevent the ocean drifting away from the given climatological mean state is to restore the sea ice cover and sea ice thickness to that found in the integration with the ECHAM5/MPI-OM. The restoring time constant is chosen as 39 days.

3 Numerical Experiments

To study the effect of fluctuating daily fluxes, three experiments were carried out. In the experiment BH, MPI-OM was driven by the climatological mean fluxes of heat, fresh water and momentum plus an additional heat flux anomaly, $H^{'}$, which was obtained from $\mathcal{B}\mathbf{y}^{'}$ with $\mathbf{y}^{'}$ representing SST anomalies. This particular form of $\mathcal{B}\mathbf{y}^{'}$ contains the SST feedbacks that prevent large climate drifts. This is shown by an additional experiment in which the MPI-OM model was driven by the fixed climatological fluxes only. The ocean drifts to a warmer climate and produces a global mean surface temperature which is about 4 °C more (not shown) than that found in the coupled ECHAM5/MPI-OM run. The drift disappears when the $\mathcal{B}\mathbf{y}^{'}$-term is installed.

In the second experiment ABC, in which all the three terms in Eq.(1) are included, the MPI-OM model was forced with the same climatological mean fluxes plus fluctuating fluxes produced by EMAD. In the third experiment AB2C, MPI-OM was coupled to EMAD with the variance of white noise doubled.

The three experiments are summarized in Tab.1. For each experiment, a spin-up run of about 600 years was carried out. The spin-up runs started from the same initial state obtained from the coupled ECHAM5/MPI-OM model (Jungclaus et al. 2005), after the ocean has reached a more or less statistically stationary state. Following the respective spin-up runs, the experiments were carried out for 200 years. The analysis given below is based on these 200-year integrations.

If all the three experiments produce the same climatological mean state (i.e. the same mean sea surface conditions and the same mean surface fluxes) and if this state is identical to that produced by the ECHAM5/MPI-OM model, the time-means of fluctuating fluxes in the three experiments will be zero. In this case, the difference between the experiments BH and ABC would describe the effect of fluctuating day-to-day fluxes, and that between the experiments BH and AB2C would describe the effect of enhanced fluctuating fluxes.

Unfortunately, the three experiments do not produce exactly the same climatological mean state of the ECHAM5/MPI-OM model. Consequently, the time-mean of fluctuating fluxes in experiments BH, ABC and AB2C are not zero. Moreover, they differ from each other, since the climatological state in experiment BH can differ from that obtained from experiment ABC or AB2C. Due to these differences, the changes from experiment BH to ABC or from BH to AB2C are induced not only by fluctuating fluxes included in experiment ABC and AB2C, but also by the differences in the time-mean fluxes. A consideration of these time-mean fluxes reveals some notable differences in the time-mean zonal wind stress (Figure 2). For instance, there is an increase in zonal wind stress in the North Atlantic (at 30°W, 50°N) and a northward shift of the mean zonal wind stress pattern over the Southern Ocean from experiment BH to experiment ABC and AB2C. The increase in zonal wind stress in the North Atlantic could be relevant, since the wind-driven gyre participates in the meridional salt transport and can therefore affect the MOC (Marti et al. 2008). The shift in the Southern Ocean could contribute to the ACC differences from experiment BH to ABC and to AB2C.

To assess the relevance of these non-zero time-mean fluxes, a supplementary experiment, referred to as BH*, is carried out. Experiment BH* is identical to experiment BH, except that the difference between the time-mean zonal wind stress of experiment BH (Figure 2a) and that of experiment ABC (Figure 2b) is added to the climatological mean wind forcing. It will be shown that the time-mean fluxes do not significantly affect the MOC changes and contribute only to a small part of ACC changes. Experiment BH* is integrated for 350 years.

4 Changes induced by fluctuating day-to-day fluxes

4.1 Time Evolutions

This subsection describes the time evolutions of the oceanic states in different experiments. The consideration is confined to the globally integrated sea surface temperature (SST) and two circulation indices, the Atlantic MOC-index and the ACC-index. The globally integrated SST is considered to describe the effect of the SST-feedback over time. The MOC-index and the ACC-index are chosen, since they characterize major global-scale circulations.

In all experiments, the SST time series are essentially statistically stationary (Figure 3a). The SST decreases slightly from experiment BH to experiment ABC and AB2C. The respective time-mean values are 18.57 °C, 18.15 °C and 18.12 °C. The spatial distribution of SST changes reveals decreases over most of the subtropical and mid-latitude oceans and increases partially over the North Atlantic from experiment BH to ABC and AB2C. The decrease is partly related to the increase in frequency and depth of convective events in the subtropical and mid-latitude oceans (see Section 4.4), which bring cold dense water down. The fluctuating fluxes also enhance the SST variability.

Figure 3b shows the time series of the MOC-index, defined as the maximum of the Atlantic meridional overturning streamfunction near 30°N at about 1220 m. The experiment BH (dotted line), which does not include fluctuating fluxes, reveals little variability in the MOC. Stronger variations are obtained by including fluctuations (solid line) in experiment ABC. The variations are strongest in experiment AB2C (dashed line) where the variance of the stochastic forcing is doubled.

Not only the variability but also the time mean of the MOC-index changes from experiment to experiment. This is further summarized in Tab.2. The smallest value of about 17 Sv is obtained from experiment BH. Inclusion of fluctuations leads to an increase of about 18 Sv in experiment ABC. Experiment AB2C, in which the strongest MOC of about 22 Sv is found, further confirms that the 1-Sv increase from experiment BH to experiment ABC is caused by the fluctuating component in the fluxes. The time-mean of the MOC-index of a 200-year time series of the coupled ECHAM5/MPI-OM simulation is also comparable to that of experiment ABC (last row in Tab.2).

Figure 3c shows the time series of the ACC-index defined as the mass transport through the Drake Passage. There is an enhancement of variability through fluctuations in experiment ABC and AB2C (solid line and dashed lines respectively). Concerning the time-mean (see also Tab.2.), a mean transport of about 200 Sv is obtained in experiment BH. This value is too high relative to the observed value of about 120 to 150 Sv (Nowlin and Klinck 1986 ; Cunningham et al. 2003). The transport reduces to about 148 Sv in experiment ABC and to about 122 Sv in AB2C.

The strength of the net mass transport through the Drake Passage reflects well the strength of the zonal current in the entire Southern Ocean (not shown). Tab.2 shows that a stronger MOC corresponds to a weaker ACC. The correspondence concerns only the time-mean values. The variability of the ACC-index is not correlated to that of the MOC-index.

To have an idea about how much of the changes listed in Tab.2 are caused by the differences in the time-mean zonal wind stress shown in Figure 2, the time-mean values of the MOC-index and the ACC-index are calculated from the last 200 years of experiment BH*. They amount to 17.2 Sv and 180 Sv, respectively. The first number suggests that the increase in zonal wind stress in the North Atlantic from Figure 2a to Figure 2b is not responsible for the 1-Sv MOC increase found by comparing experiment ABC with experiment BH. Instead, the 1-Sv increase is likely caused by the fluctuating fluxes included in experiment ABC. The second number suggests that the ACC change from experiment BH to ABC is partly due to the northward shift in the time-mean zonal wind stress shown in Figure 2b. However, if the effect of time-mean wind stress and that of fluctuating fluxes can be linearly superimposed, the effect due to the time-mean zonal wind stress is smaller than that of the fluctuating fluxes.

For the comparison, the values of the MOC- and ACC-indices in ECHAM5/MPI-OM are shown in Tab.2 (last row). If the climatological mean state in the ECHAM5/MPI-OM model is identical to that in the hybrid EMAD/MPI-OM model, the values obtained from experiment ABC would be close to those shown in the last row. One finds a good agreement for the MOC-index, but not as good an agreement for the ACC-index. This further confirms that the circulation in the MPI-OM model is more sensitive to the time-mean zonal wind stresses in the Southern Ocean than those in the North Atlantic.

4.2 Changes in the Atlantic Meridional Overturning Circulation

The different formulations of the surface fluxes result in different Atlantic meridional overturning circulations (Figure 4). The difference concerns not only the strength that is described by the MOC-index in Figure 3 and Tab.2., but also the structure. When the MPI-OM is driven by the climatological fluxes plus the oceanic feedbacks (experiment BH), an overturning cell of around 2800 m and 17 Sv maximum strength is obtained (Figure 4a). In experiment ABC (Figure 4b), the overturning cell is stronger and extends a couple of hundreds of meters down to the deep ocean compared to that of BH. When the stochastic forcing is doubled, the overturning circulation further strengthens and deepens (Figure 4c). The deepening of the overturning cell is accompanied by the weakening of the Antarctic Bottom Water cell and the retreat of the Antarctic Bottom Water (AABW). In experiment AB2C, the penetration of AABW into the abyssal North Atlantic is severely blocked. The spatial structure of the Atlantic MOC in experiment ABC is comparable to that produced by the ECHAM5/MPI-OM model (not shown) and that obtained from an ensemble of coupled AOGCMs (Stouffer et al. 2006).

To make sure that the 1-Sv increase in MOC is statistically significant, a t-test is carried out. The null hypothesis that the maximum overturning in experiment BH equals that in experiment ABC is considered. The null hypothesis is rejected with 1% risk.

To show that the above described structural changes do not result from the different time-mean zonal wind stress, the mean Atlantic overturning streamfunction obtained from the last 200 years of experiment BH* is shown in Figure 5. Both the strength and the structure are comparable to the streamfunction obtained from experiment BH.

4.3 Changes in the density fields

To understand whether and to what extent fluctuating fluxes change the mean circulation via changing density structures, consider first the situation at the surface. Figure 6a shows the zonal-mean meridional profiles of surface density in the Atlantic sector. The large differences at the high northern latitudes result from different climatological mean states in the Arctic: the Arctic becomes more saline from experiment BH to experiment ABC and AB2C (not shown). In the North Atlantic from about 40°N to 75°N, it is difficult to relate changes in the meridional density gradient to the MOC changes found in experiments BH, ABC and AB2C. In the south from 30°S to 60°S, the meridional gradient in experiment BH is stronger than that in experiment ABC and AB2C, as indicated by the dotted line (BH) which is below the solid (ABC) and dashed (AB2C) lines north of about 45°S and above them, south of 45°S. The change from experiment ABC to AB2C (solid and dashed lines) is less clear. Following the previous studies (e.g. Russell et al. 2006) suggesting that the ACC is related to the density gradient in deeper layers, in particular to the density gradient integrated over the sill depth, density changes in the oceanic interior were considered.

Indeed the effects of fluctuating fluxes can be traced down to the deep ocean. Figure 7a shows the in-situ density in experiment BH at 1365 m. The density field is characterized by higher density in the Atlantic and the Southern Oceans than in the Pacific and the Indian Oceans. To describe the changes in the density gradient induced by fluctuating fluxes, the differences between experiments ABC and BH and between AB2C and BH are shown in Figure 7b and c, respectively. The dominant feature of the density changes is the zonally oriented density increases centered near 40°S and density decreases further south. The amplitudes of the density increases are larger than those of decreases. These changes lead to a reduction in the meridional density gradient in the Southern Ocean and hence a weakening of the ACC.

The density changes in the North Atlantic are more subtle. From the difference AB2C-BH shown in Figure 7c, one can identify a few isolines in the Atlantic north of 40°N that reveal strong tilt in the north-south direction. These isolines suggest an increase in the zonal density gradient that are by geostrophic relation consistent with the large increase of the MOC of more than 4 Sv from experiment BH to AB2C. However, this feature does not show up clearly in the difference ABC-BH (Figure 7b).

A further search for a clear relation between changes in density distribution and changes in the Atlantic MOC leads to the consideration of the depth-integrated in-situ density. This quantity was shown to be related to the strength of the MOC in previous studies (Hughes and Weaver, 1994 and Thorpe et al 2001). Figure 6b shows the zonal mean of depth-integrated in-situ density in the Atlantic sector. The increase of the density equatorward of about 40° from experiment BH to ABC and AB2C is related to the change in the climatological mean state, which becomes colder in experiment ABC and AB2C, relative to that in experiment BH. The cooling is partly due to the increase in frequency and depth of convective events (see Section 4.4). Regarding the meridional gradient, the meridional gradients between 40°S and 40°N and between 40°N and 60°N do not change much. However, small changes in density difference between northern North Atlantic and the South Atlantic are possible. After calculating the density difference between different latitudinal strips in the North and South Atlantic, we found that the density difference between the northern strip extending from 55°N to 60°N and the southern strip extending from 45°S to 50°S increases with the MOC from 0.11 kg/m^3 in experiment BH to 0.12 kg/m^3 in experiment ABC and to 0.13 kg/m^3 in experiment AB2C. A similar north-south density difference was considered in studies by Rahmstorf (1996) and Thorpe et al (2001).

In the Southern Ocean, the meridional gradient of the depth-integrated density (Figure 6b) is reduced. Expressed in terms of the density difference between 40°S and 60°S, one finds decreases from 1.02 kg/m^3 in experiment BH (dotted) to 0.77 kg/m^3 in experiment ABC (solid) and to 0.63 kg/m^3 in experiment AB2C (dashed).

The reduction of meridional gradient is more strongly related to the increase in density around 40°S than to the decrease in density around 60°S. These changes in meridional density distribution are related to the changes in ACC in different experiments by the geostrophic relation.

4.4 Changes in the vertical mixing

In this section, the way surface fluxes alter the density in the deep ocean is examined. It will be shown that surface fluxes change the density via vertical mixing. Before dealing with these mixing changes, consider first the time-mean mixing, as described by the time-mean vertical diffusion coefficient K for experiment BH at 285 m depth in Figure 8a and at 900 m depth in Figure 9a. In GIN Seas and along and near the Antarctic coast in the Atlantic sector and south of the South America, large time-mean values of K and mean convection depth (Figure 10a) are found, which is also the case in the coupled ECHAM5/MPI-OM model. These regions are the most unstable regions of the ocean model. Elsewhere, the modelled ocean is much more stable.

A maximum of K is also found at 285 m in the north Pacific just west of the date line between 50°N and 60°N (Figure 8a). This maximum disappears at 900 m in Figure 9a. The map of the mean depth of convection (Figure 10a) suggests that the convection related to this maximum is shallower than 600-650 m.

Generally, K is smaller than 0.002 m^2/s in most part of the ocean at 900 m and decreases with depth to values smaller than 10^{-4} m^2s^{-1} below 2500 m. These values should be compared with the observational range of 10^{-6} to 10^{-3} m^2/s reported from interior oceanic regions (Ledwell et al. 1993; Moum et al. 2002, Gregg et al. 2003, Ledwell et al. 2000, Sloyan 2005).

Consider now the changes in the vertical mixing due to different surface fluxes. In the following, the effect of the fluctuating fluxes is indicated by the difference in K (ABC-BH) obtained from experiment ABC and BH. The effect of the fluctuations with enhanced variance is obtained by comparing the difference AB2C-BH with the difference ABC-BH. The possible effect of the time-mean zonal wind stress on changes in K is small and will be discussed at the end of this section.

Figure 8b shows the difference in K (ABC-BH) at 285 m depth, induced by the fluctuations. Outside the tropics, where large changes of K are found, there is a striking correspondence between the distribution of the time-mean frequency and depth of convective events shown in Figure 8a and Figure 10a and the distribution of the changes in K from experiment BH to ABC shown in Figure 8b in the MPI-OM model: The strong decreases in K are found in the regions where the time-mean values of K are large, indicating frequent occurrence of convective events due to mostly unstable stratification. These regions consist of the GIN Seas, an area centered near 50°W and 35°N in the North Atlantic, the areas south of the South American continent and west and east of the Antarctic Peninsula. The increases in K, on the other hand, are found in regions where the time-mean values of K are generally small and convective events are less frequent due to mostly stable stratification. In the North Atlantic, an area with increases in K is found between

40°N to 60°N, south of the GIN Seas. There, the time-mean values of K are generally small, apart from the areas close to the Irminger Sea which will be discussed at the end of this section. In the Southern Ocean, increases in K are found mainly in the latitude band from 20°S to 50°S. This correspondence between the time-mean values of K and changes in K can also be seen in experiment AB2C (Figure 8c).

At 900 m (Figure 9b), the correspondence between the time-mean mixing and the changes in the convective mixing is also noticeable poleward of about 40°. In particular, the decreases in K are mainly located in regions with large values of the time-mean mixing shown in Figure 9a. Overall, the magnitudes of mixing changes are much smaller at 900 m (Figure 9b,c) than at 285 m (Figure 8b,c). The areas with enhanced mixing in experiment ABC (Figure 9b) is enlarged when the strength of stochastic fluctuations is doubled in experiment AB2C (Figure 9c): The patchy structure over the Southern Ocean in Figure 9b becomes more uniform in Figure 9c. Mixing structures similar to Figure 9 but with smaller amplitudes can be found down to about 2500 to 3000 m. Further below, the mixing signal is much less zonally oriented.

Following the definition of K, the above described changes in K are related to changes in the *frequency* of convective events. Changes in the mean *depth* of convective events are described in Figure 10b and c. The largest changes in the mean convection depth are about 300 m. A comparison of Figure 10b,c with Figure 8b,c suggests that, apart from the tropical oceans, an increase (a decrease) in the frequency of convective events corresponds to an increase (a decrease) in the depth of convective events. Since the regions with small (large) time-mean values of K and shallow (deep) mean convection represent regions which are often stably (unstably) stratified, one can conclude that the fluctuating fluxes tend to increase the convective mixing over mostly stable ocean and decrease convective mixing over mostly unstable ocean. Moreover, an increase (a decrease) in convective mixing is accomplished by an increase (a decrease) in both frequency and depth of convective events.

The above described mixing changes can be responsible for the density changes described in Section 4.3. As the enhanced vertical mixing is related to an increase in the frequency and the depth of convective events and these events generally bring dense water down, the increase in vertical mixing in the midlatitudes found in experiments ABC and AB2C can lead to an increase in density there. In the Atlantic, the increase in the vertical mixing near the northern strip 55°N-60°N is stronger than that in the southern strip 45°S-50°S. This can lead to the increase of the density difference between the two strips from experiment BH to experiment ABC and AB2C, which is related to the respective MOC increases. The large-scale increase in the vertical mixing in the Southern Ocean can be responsible for the increase in density near 40°S, which results in a weaker meridional density gradient and a weaker ACC.

There exists a few spots where the change in K is not clearly related to the mean stratification, for instance west of Svalbard and also in the Arctic.

Note that the distribution of changes in the convection depth (Figure 10b, c) compares less well with changes in K at 900 m (Figure 9b, c) than with changes at 285 m (Figure 8b, c). This is because Figure 10 represents the mean convection depth, rather than the depth of individual convective events. Apart from a few exceptions at high-latitudes, convective events are mostly shallower than a few hundred meters. The changes in convection depth due to fluctuating fluxes are generally smaller than 300 m. Thus, Figure 10b and c reflect mainly the changes related to convections shallower than 900 m.

Also in tropical oceans, the changes in convective activity (Figure 10b,c) do not correspond to changes in K (Figure 8b,c and Figure 9b,c) in tropical oceans. There, one finds increases in the convective depth, even though the vertical mixing is reduced. This is because convective events are confined to the upper 60 m in the tropical and subtropical Atlantic and Indian Oceans and to the upper 100 m in the tropical and subtropical Pacific, but can reach a few hundred meters in the extra-tropical regions. As the convective events triggered by the fluctuating daily fluxes are confined to a shallow surface layer, the decrease in K in the tropics below, say, 100 m, as seen in Figure 8b,c and Figure 9b,c is likely caused by the Ri-dependent mixing, rather than the convective mixing.

The above described mixing changes are mainly due to fluctuating fluxes. The effect of time-mean fluxes is mostly secondary. This is shown by the difference in the mean convection depth found in the experiments ABC and BH* (Figure 11). Different from Figure 10b which shows changes due to fluctuating fluxes *and* the difference in the time-mean zonal wind stress, the effect due to different time-mean zonal wind stress is eliminated in Figure 11. Since Figure 10b is very close to

Figure 11, the effect due to different time-mean zonal wind stress must be small. An exception is the change near the Irminger Sea. In this region, the mechanism which alters the MOC through the wind-driven gyre (Marti et al. 2008) can be at work. The stronger time-mean zonal wind stress in experiment ABC can transport more salt northward, whereby enhancing the surface density and triggering more often convective events. This is likely the reason, why large increases in the frequency and depth of convective events are found in the Irminger Sea (Figure 8b and Figure 10b), where, if the effect of fluctuating fluxes dominated, a decrease in the frequency and depth of convective events was expected.

5 Conclusions and discussion

The MPI-OM model coupled to the empirical flux model EMAD is used to isolate the effect of fluctuating fluxes. It is found that fluctuating daily fluxes can produce a 1-Sv-increase in the strength of the Atlantic MOC, which is about 7% of the MOC obtained without the fluctuating fluxes, and a 32-Sv-reduction of the ACC, which is about 16% of the ACC obtained without fluctuating fluxes. These changes exclude (with the aid of experiment BH*) the effect of non-zero time-mean fluxes that cannot be completely excluded from the experiments. The MOC changes are related to the change in the meridional density difference between two latitudinal strips in the northern North Atlantic and in the South Atlantic, defined in a way similar to that in Rahmstorf (1996) and Thorpe et al (2001). The ACC changes are related to a reduction in meridional gradient in the depth-integrated density.

These density changes are likely caused by changes in vertical mixing induced by fluctuating surface fluxes. In the MPI-OM model, large changes in the vertical mixing are related to the changes in the convective mixing. Fluctuating fluxes alter convective mixing in a non-linear way. In the mostly unstable regions, e.g. in the GIN Seas and near the Antarctic Peninsula, positive buoyancy anomalies can restrain convective events, whereas negative buoyancy anomalies do not significantly affect the convective behaviour, leading to an overall reduction in the convective mixing. In mostly stable regions, e.g. in the subtropical and mid-latitude oceans, large negative buoyancy anomalies can trigger additional convective events, whereas positive buoyancy anomalies do not significantly change the convective behaviour, leading to an overall strengthening of the convective mixing.

The conclusions about the effect of fluctuating fluxes on the convective mixing are drawn within the framework of a coarse resolution version of the MPI-OM. In another OGCM, which produces a different stratification with a different distribution of convective activity, the effect of fluctuating fluxes on the convective mixing, which is closely related to the mean stratification, can be different. As a consequence, the exact numbers concerning the changes in the MOC and ACC due to the fluctuating fluxes can depend on the model used. Nevertheless, the mechanism through which fluctuating daily fluxes alter the convective mixing should operate in other models, and probably also in nature.

ACKNOWLEDGMENTS

This study is supported by the German Research Foundation in the Special Research Areas (SFB 512), “Cyclones and the North Atlantic Climate System”. We thank Uwe Mikolajewicz and two anonymous reviewers for valuable suggestions in improving this manuscript. Thanks also to Johann Jungclaus who provided us a program to calculate the volume transports between the Nordic Seas and the North Atlantic which helped us to answer a question raised by a reviewer.

REFERENCES

Cunningham S, Alderson S, King BA, Brandon MA (2003) Transport and variability of the ACC. J Geophys Res 108. doi:10.1029/2001JC001147

Frankignoul C, Czaja A, L'Heveder B (1998) Air-sea feedback in the North Atlantic and surface boundary conditions for ocean models. J Clim 11:2310-2324

Gent PR, Willebrand J, McDougall J, McWilliams JC (1995) Parameterising eddy induced tracer transports in ocean circulation models. J Phys Oceanogr 25:463-474

Gregg M, Sanford T, Winkel D (2003) Reduced mixing from the breaking of internal waves in equatorial waters. Nature 422:513-515

Griffies SM (1998) The Gent-McWilliams skew flux. J Phys Oceanogr 28:831-841

Haak H, Jungclaus JH, Mikolajewicz U, Latif M (2003) Formation and propagation of great salinity anomalies. Geophys Res Lett 30. doi:10.1029/2003GL017065

Hughes T, Weaver A (1994) Multiple equillibrium of an asymmetric two-basin model. J Phys Oceanogr 24:619-637

Jungclaus JH, Haak H, Latif M, Mikolajewicz U (2005) Arctic-North Atlantic interactions and multidecadal variability of the meridional overturning circulation. J Clim 18:4013-4031

Kuhlbrodt T, Griesel A, Montoya M, Levermann A, Hoffmann M, Rahmstorf, S

(2007) On the driving processes of the oceanic meridional overturning circulation. Rev Geophys 45. doi:10.1029/2004RG000166

Kuhlbrodt T, Monahan A (2003) Stochastic stability of open-ocean deep convection. J Phys Oceanogr 33:2764-2780

Ledwell J, Montgomery E, Polzin K, St.Laurent, Schmitt L, Toole J (2000) Evidence for enhanced mixing over rough topography in the abyssal ocean. Nature 403:179-182

Ledwell J, Watson A, Law C (1993) Evidence for slow mixing across the pycnocline from an open-ocean tracer release experiment. Nature 364:701-703

Legutke S, Voss R (1999) The Hamburg atmosphere-ocean coupled circulation model ECHO-G. DKRZ, Tech. Rep. 18, Hamburg, Germany

Marsland SJ, Haak H, Jungclaus JH, Latif M, Roeske F (2003) The Max-Planck-Institute global ocean/sea ice model with orthogonal curvilinear coordinates. Ocean Model 5:91-127

Marti O, Braconnot P, Dufresne J-L, Bellier J, Benshila R, Bony S, Brockmann P, Cadule P, Caubel A, Codron F, de Noblet N, Denvil S, Fairhead L, Fichefet T, Foujols M-A, Friedlingstein P, Goosse H, Grandpeix J-Y, Guilyardi E, Hourdin F, Krinner G, Lvy C, Madec G, Mignot J, Musat I, Swingedouw D, Talandier C (2009) Key features of the IPSL ocean atmosphere model and its sensitivity to atmospheric resolution. Clim Dyn (submitted)

Moum J, Caldwell D, Nash J , Gunderson G (2002) Observations of boundary mixing over the continental slope. J Phys Oceanogr 32:2113-2130

Munk W, Wunsch C (1998) Abyssal recipies II. Energetics of tidal and wind mixing. Deep Sea Res I 45:1977-2010

Nowlin WDJ, Klinck JM (1986) The physics of the ACC. Rev Geophys 24:469-491

Pacanowski RC, Philander SGH (1981) Parameterisation of vertical mixing in numerical models of tropical oceans. J Phys Oceanogr 11:1443-1451

Rahmstorf S (1995) Multiple convection patterns and thermohaline flow in an idealized OGCM. J Clim 8:3028-3039

Rahmstorf S, Willebrand J (1995) The role of temperature feedback in stabilizing the thermohaline circulation. J Phys Oceanogr 25:787-805

Rahmstorf S (1996) On the freshwater forcing and transport of the Atlantic thermohaline circulation. Clim Dyn 12:799-811

Raible C, Luksch U, Fraedrich K, Voss R (2001) North Atlantic decadal regimes in a coupled GCM simulation. Clim Dyn 18:321-330

Redi MH (1982) Oceanic isopycnal mixing by coordinate rotation. J Phys Oceanogr 12:1154-1158

Russell JL, Stouffer RJ, Dixon KW (2006) Intercomparison of the southern ocean circulations in IPCC coupled model control simulations. J Clim 19:4560-4575

Sloyan BM (2005) Spatial variability of mixing in the Southern Ocean. Geophys Res Lett 32. doi:10.1029/2005GL023568

Stouffer RJ, Yin J, Gregory JM, Dixon KW, Spelman MJ, Hurlin W, Weaver AJ, Eby M, Flato GM, Hasumi H, Hu A, Jungclaus JH, Kamenkovich IV, Levermann A, Montoya M, Murakami S, Nawrath S, Oka A, Peltier WR, Robitaille DY, Sokolov A, Vettoretti G, Webber SL (2006) Investigating the causes of the response of the thermohaline circulation to past and future climate changes. J Clim 19:1365-1387

Swingedouw D, Braconnot P, Delecluse P, Guilyardi E, Marti O (2007) Quantifying the AMOC feedbacks during a 2xCO2 stabilization experiment with land - ice melting. Clim Dyn 29:521-534

Thorpe RB, Gregory JM, Johns TC, Wood RA, Mitchell JFB (2001) Mechanisms determining the Atlantic thermohaline circulation response to greenhouse gas forcing in a non-flux adjusted coupled climate model. J Clim 14:3102-3116

Toggweiler JR, Samuels B (1995) Effect of Drake Passage on the global thermohaline circulation. Deep Sea Res 42:477-500

Tziperman E (1986) On the role of interior mixing and air sea fluxes in determining the stratification and circulation of the oceans. J Phys Oceanogr 16:680-693

von Storch J-S (2000) Signatures of air-sea interactions in a coupled atmosphere-ocean GCM. J Clim 13:3361-3379 von Storch J-S, Montavez JP, Beena BS (2005) EMAD: An empirical model of air-sea fluxes. Meteor Zeitschrift 14:755-762

Walin G (1982) On the relation between sea-surface heat flow and thermal circulation in the oceans. Tellus 34:187-195

Webb DJ, Suginohara N (2001) Vertical mixing in the ocean. Nature 409:37

FIGURE CAPTIONS

Figure 1: Daily snapshots of wind stress and heat flux anomalies from a) EMAD model and b) NCEP/NCAR Reanalysis. The units are in $Pascal$ and W/m^2 respectively.

Figure 2: Time-mean zonal wind stress in Pa obtained in a) experiment BH, b) experiment ABC and c) experiment AB2C.

Figure 3: Yearly time series of a) globally integrated sea surface temperature in ^oC, b) the maximum of Atlantic meridional overturning streamfunction located near 30°N in Sv (MOC-index) and c) Drake Passage mass transport in Sv (ACC-index) obtained from experiment BH (dotted), ABC (solid) and AB2C (dashed).

Figure 4: Spatial structure of the time-mean Atlantic MOC in Sv in different experiments.

Figure 5: Spatial structure of the time-mean Atlantic MOC in Sv in experiment BH*.

Figure 6: Meridional profiles of the zonal mean of surface density and the zonal mean of depth-integrated in-situ density in the Atlantic sector obtained from experiment BH (dotted), ABC (solid) and AB2C (dashed). The depth integration starts from 1220 m for experiments BH, ABC and AB2C. The Atlantic sector covers the oceanic region from 70°W to 10°E and hence includes the Drake passage. Unit is kg/m^3.

Figure 7: Horizontal distributions of in situ density at 1365 m in kg/m^3 for a) the time-mean in experiment BH and b) the difference between experiments ABC and BH and c) between experiments AB2C and BH.

Figure 8: Horizontal distributions of K at 285 m in m^2/s for a) the time-mean in experiment BH and b) the difference between experiments ABC and BH and c) between experiments AB2C and BH.

Figure 9: Same as Figure 8, but for K at 900 m.

Figure 10: Horizontal distributions of mean convection depth in m for a) the time-mean in experiment BH and b) the difference between experiments ABC and BH and c) between experiments AB2C and BH.

Figure 11: Horizontal distribution of the change in the mean convection depth in m between experiments ABC and BH*.

TABLE CAPTIONS

Table 1 : Experiments done with MPI-OM driven by different types of daily fluxes at the sea surface. $\bar{\mathbf{x}}$ denotes the climatological fluxes and $\mathbf{x}'$ the flux anomalies predicted by different versions of EMAD model.

Table 2 : 200-year means of MOC-index and ACC-index in Sv in different experiments.

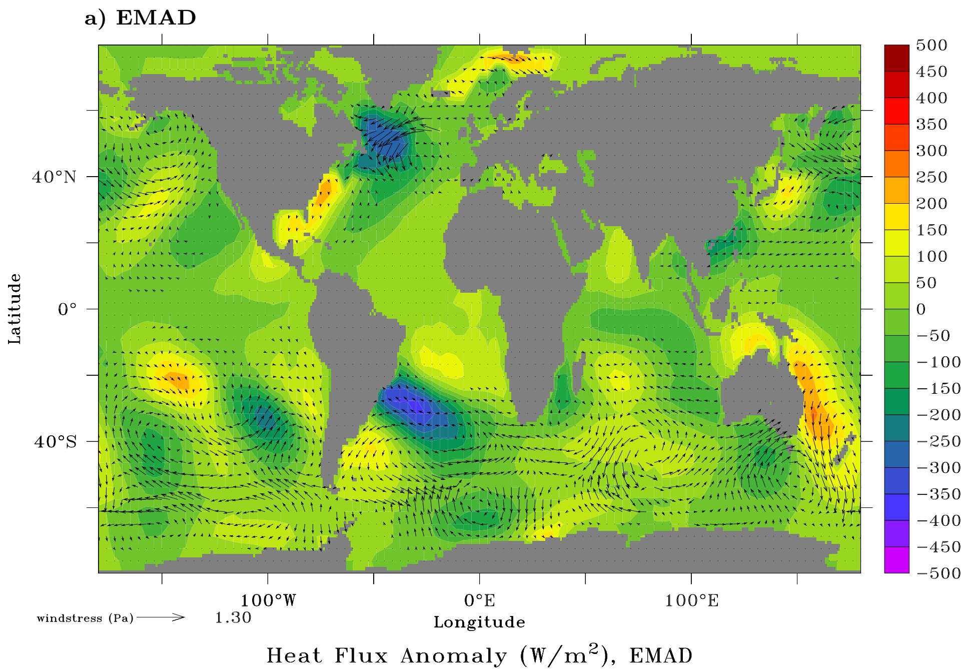

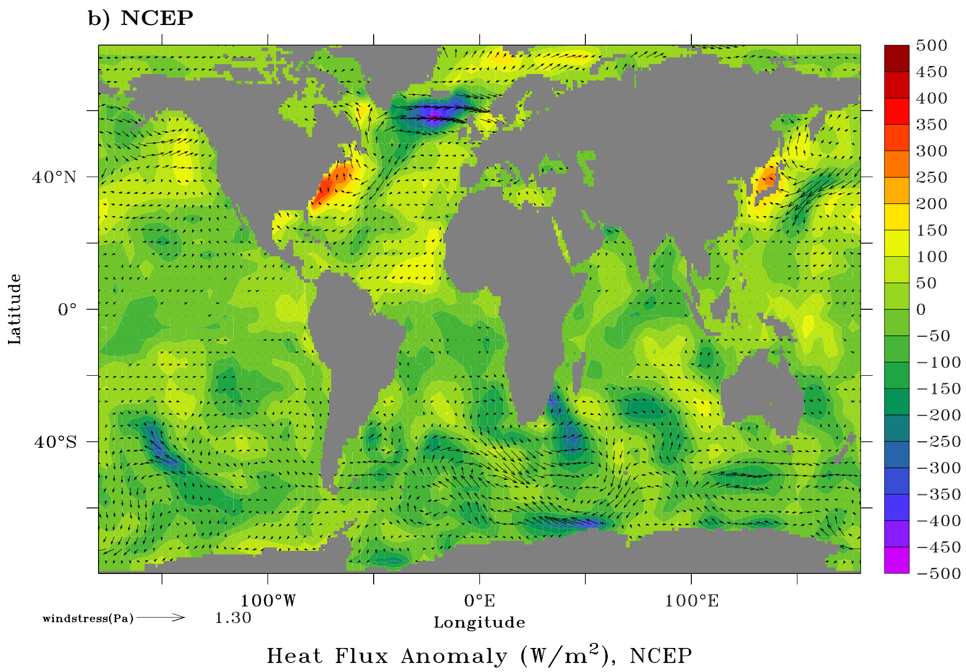

Figure 1: Daily snapshots of windstress and heatflux anomalies from a) EMAD model and b) NCEP/NCAR Reanalysis. The units are in $Pascal$ and W/m^2 respectively.

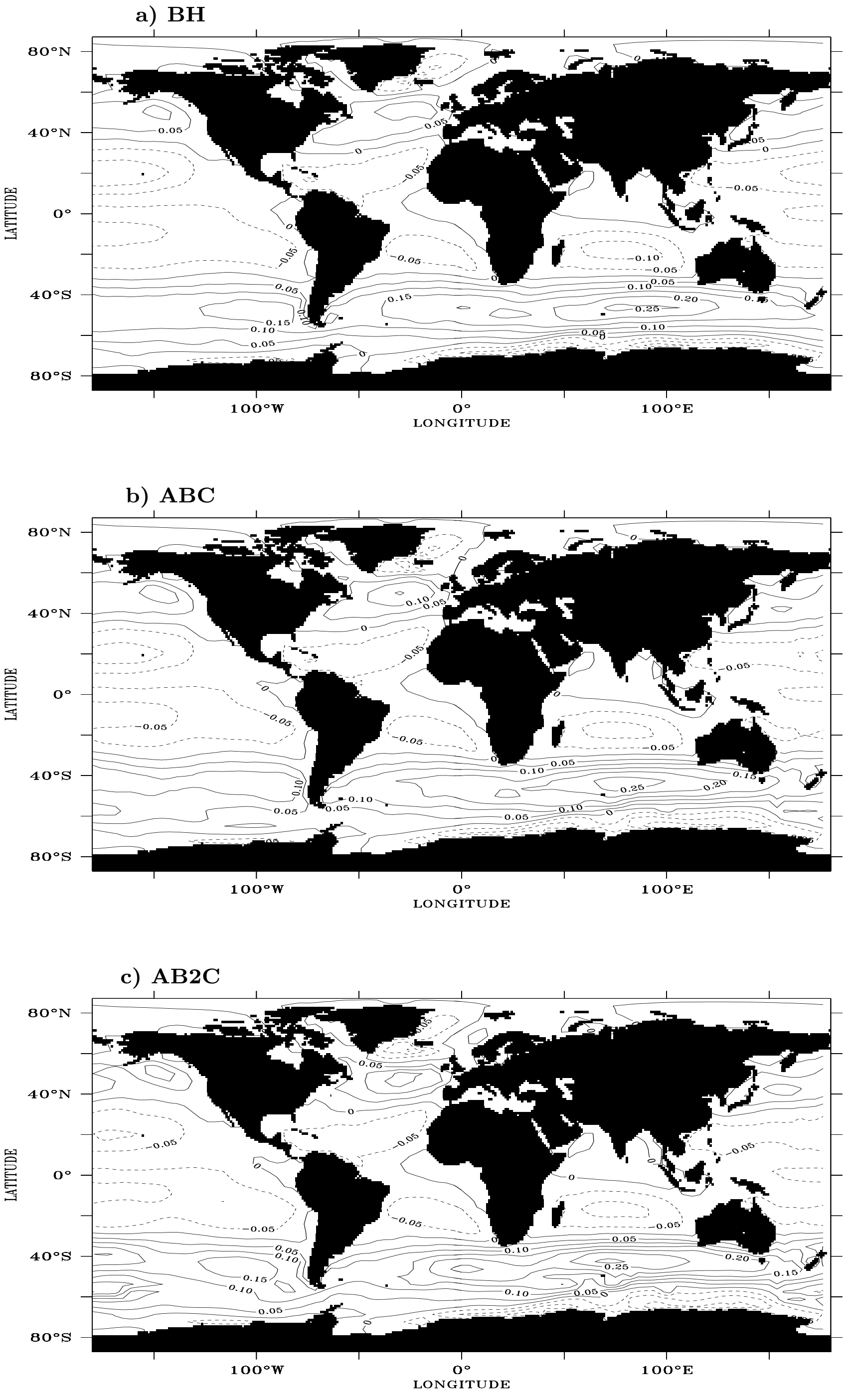

Figure 2: Time-mean zonal wind stress in Pa obtained in a) experiment BH, b) experiment ABC and c) experiment AB2C.

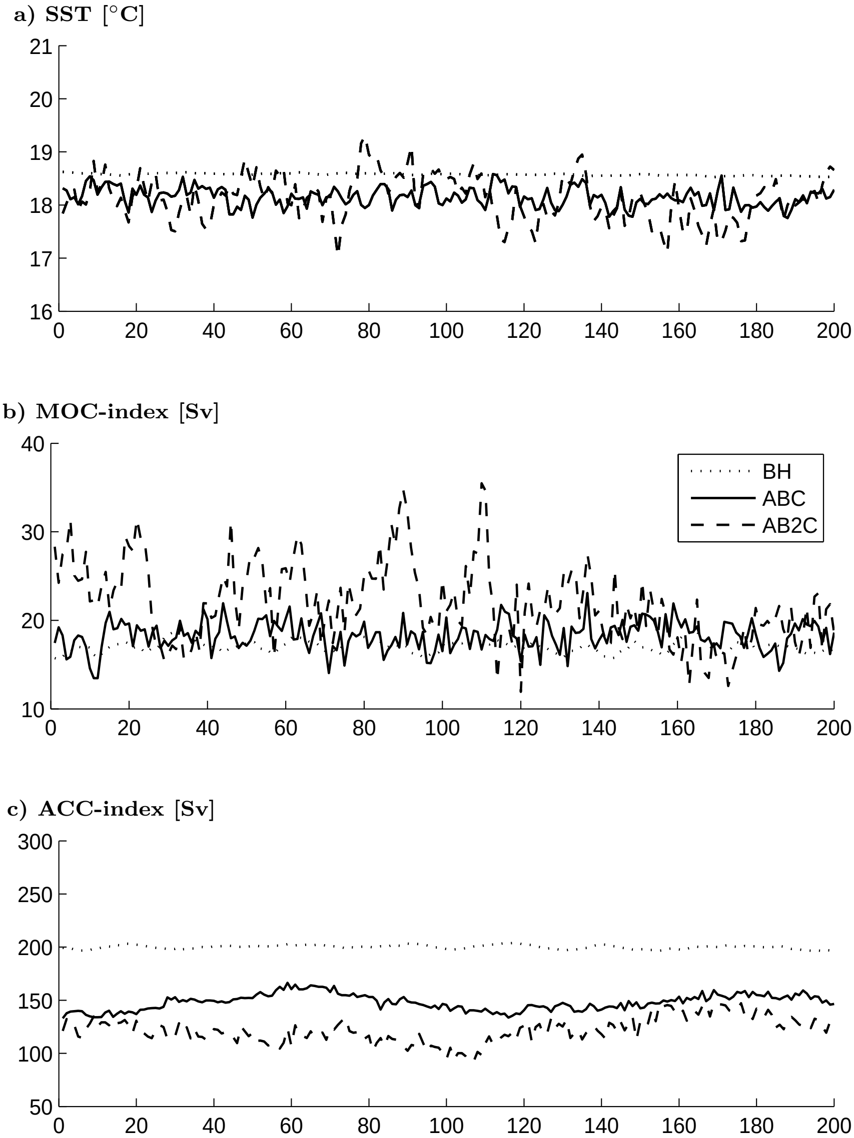

Figure 3: Yearly time series of a) globally integrated sea surface temperature in ^oC, b) the maximum of Atlantic meridional overturning streamfunction located near 30°N in Sv (MOC-index) and c) Drake Passage mass transport in Sv (ACC-index) obtained from experiment BH (dotted), ABC (solid) and AB2C (dashed).

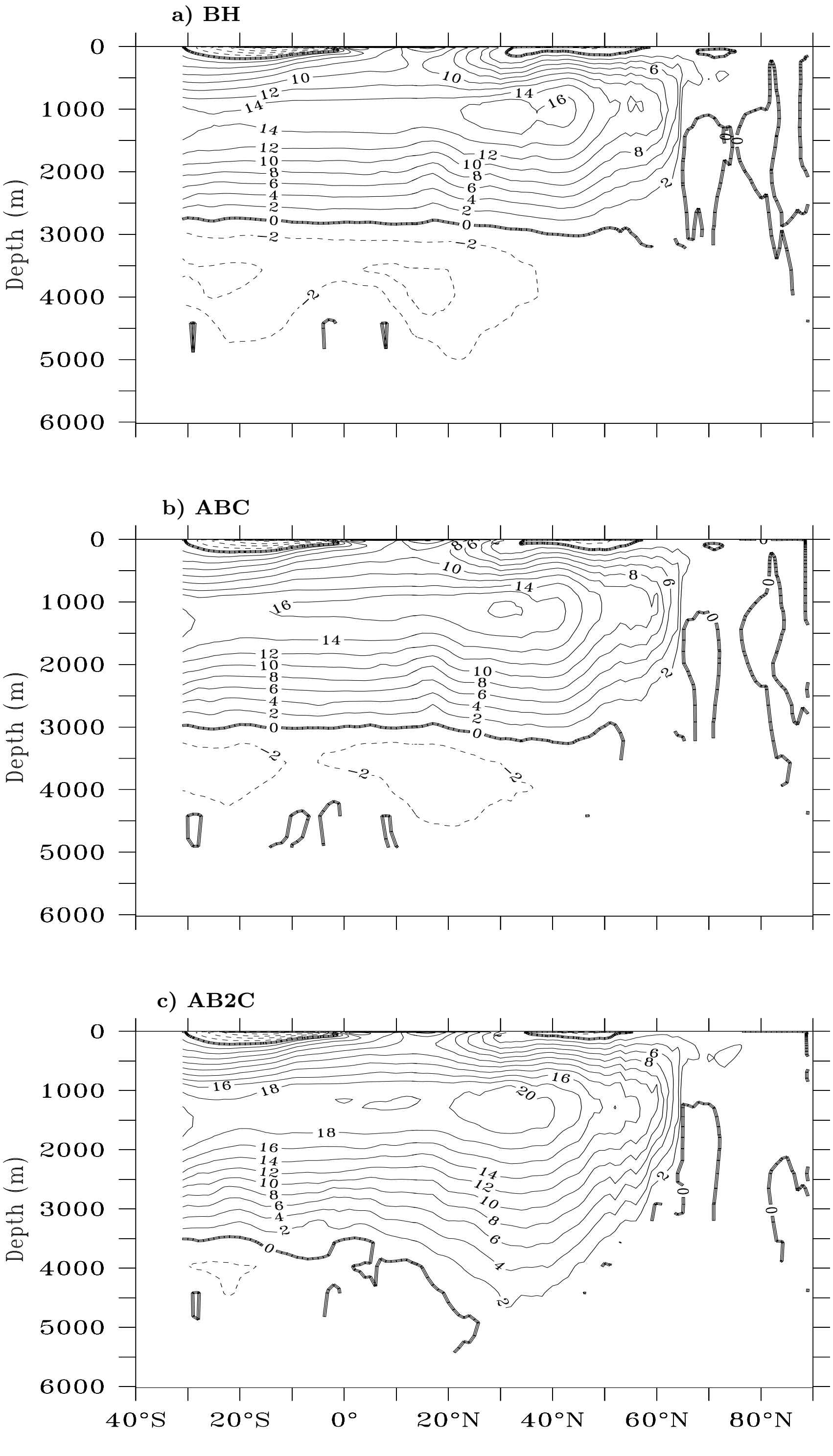

Figure 4: Spatial structure of the time-mean Atlantic MOC in Sv in different experiments.

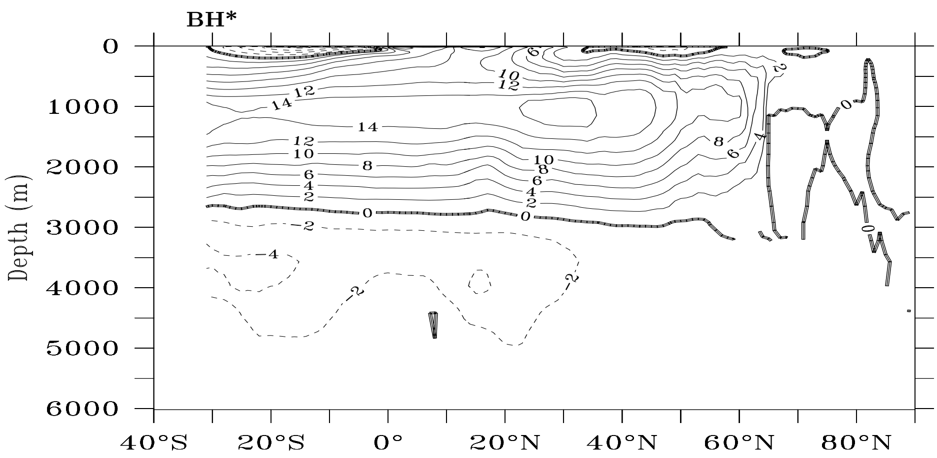

Figure 5: Spatial structure of the time-mean Atlantic MOC in Sv in experiment BH*.

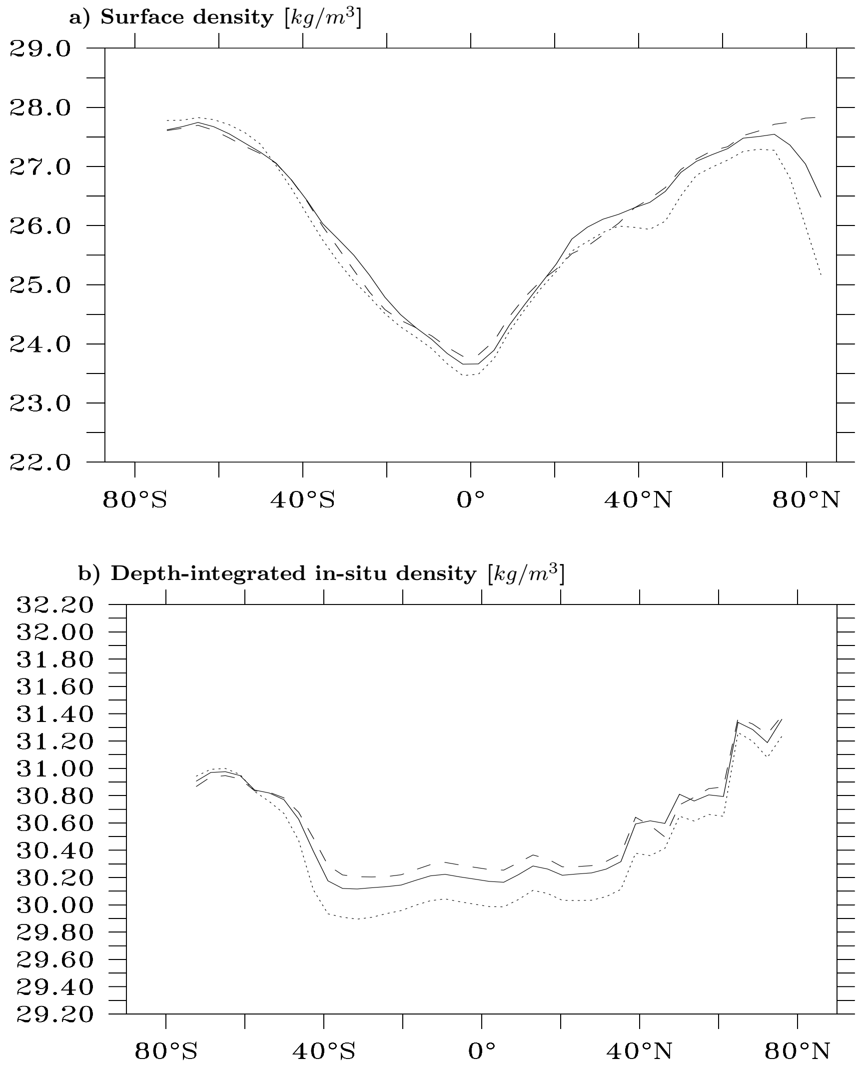

Figure 6: Meridional profiles of the zonal mean of surface density and the zonal mean of depth-integrated in-situ density in the Atlantic sector obtained from experiment BH (dotted), ABC (solid) and AB2C (dashed). The depth integration starts from 1220 m for experiments BH, ABC and AB2C. The Atlantic sector covers the oceanic region from 70°W to 10°E and hence includes the Drake passage. Unit is kg/m^3.

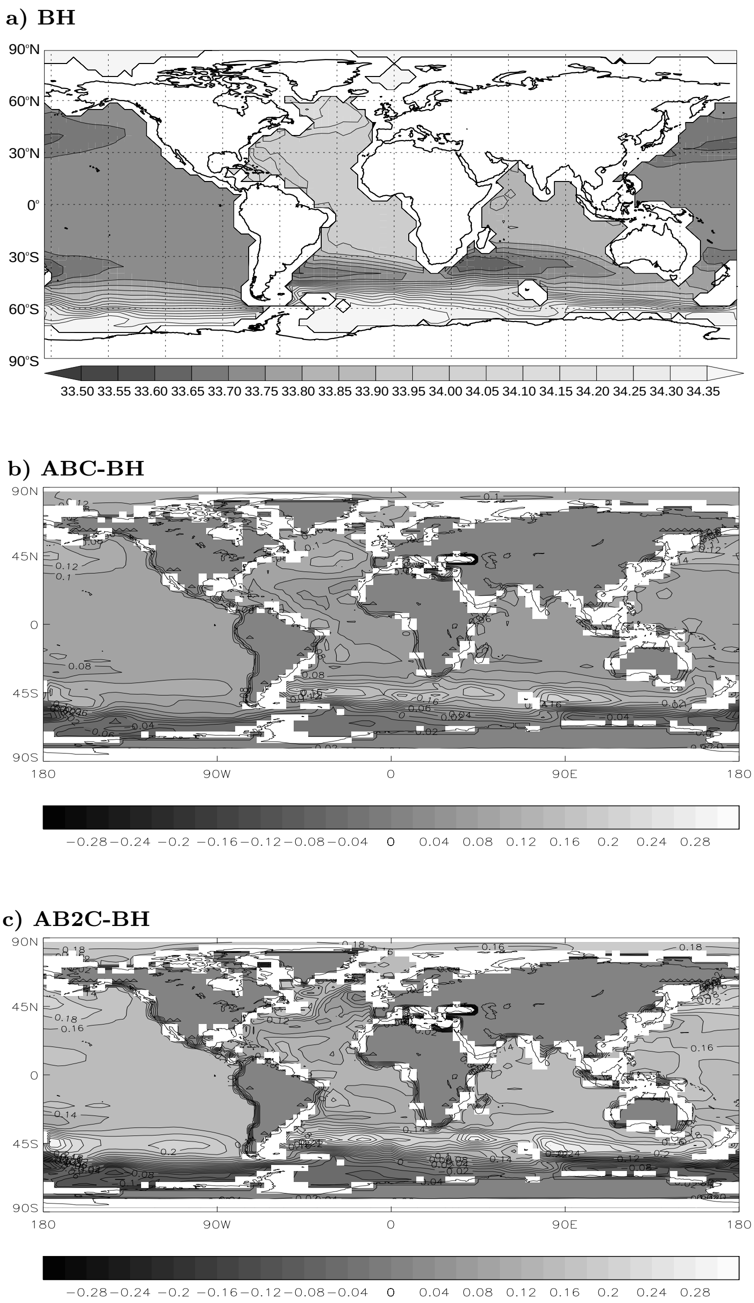

Figure 7: Horizontal distributions of a) the time-mean in situ density at 1365 m in experiment BH and b) the difference between density in experiments ABC and BH and c) between experiments AB2C and BH. The unit is kg/m^3.

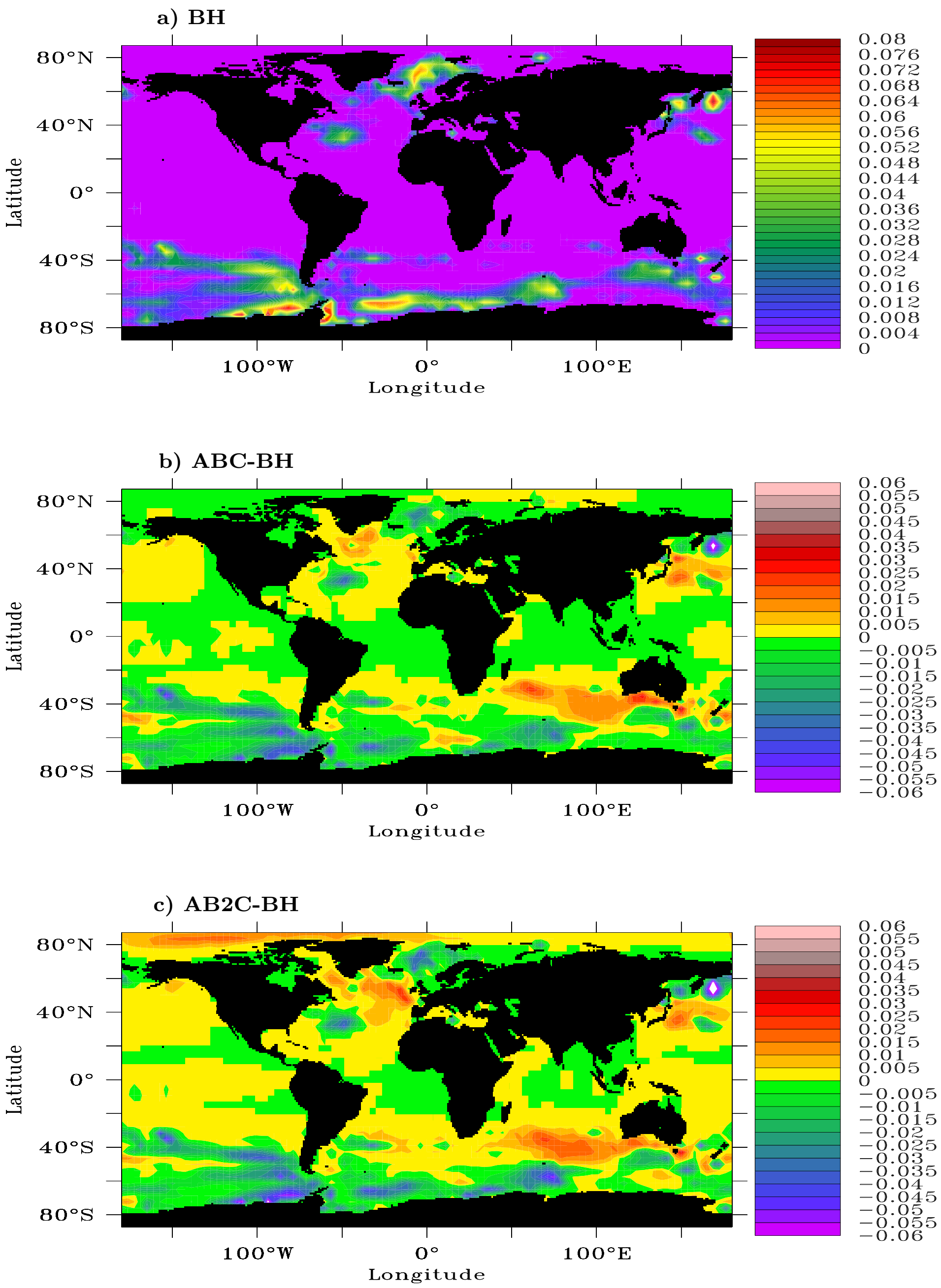

Figure 8: Horizontal distributions of K at 285 m in m^2/s for a) the time-mean in experiment BH and b) the difference between experiments ABC and BH and c) between experiments AB2C and BH.

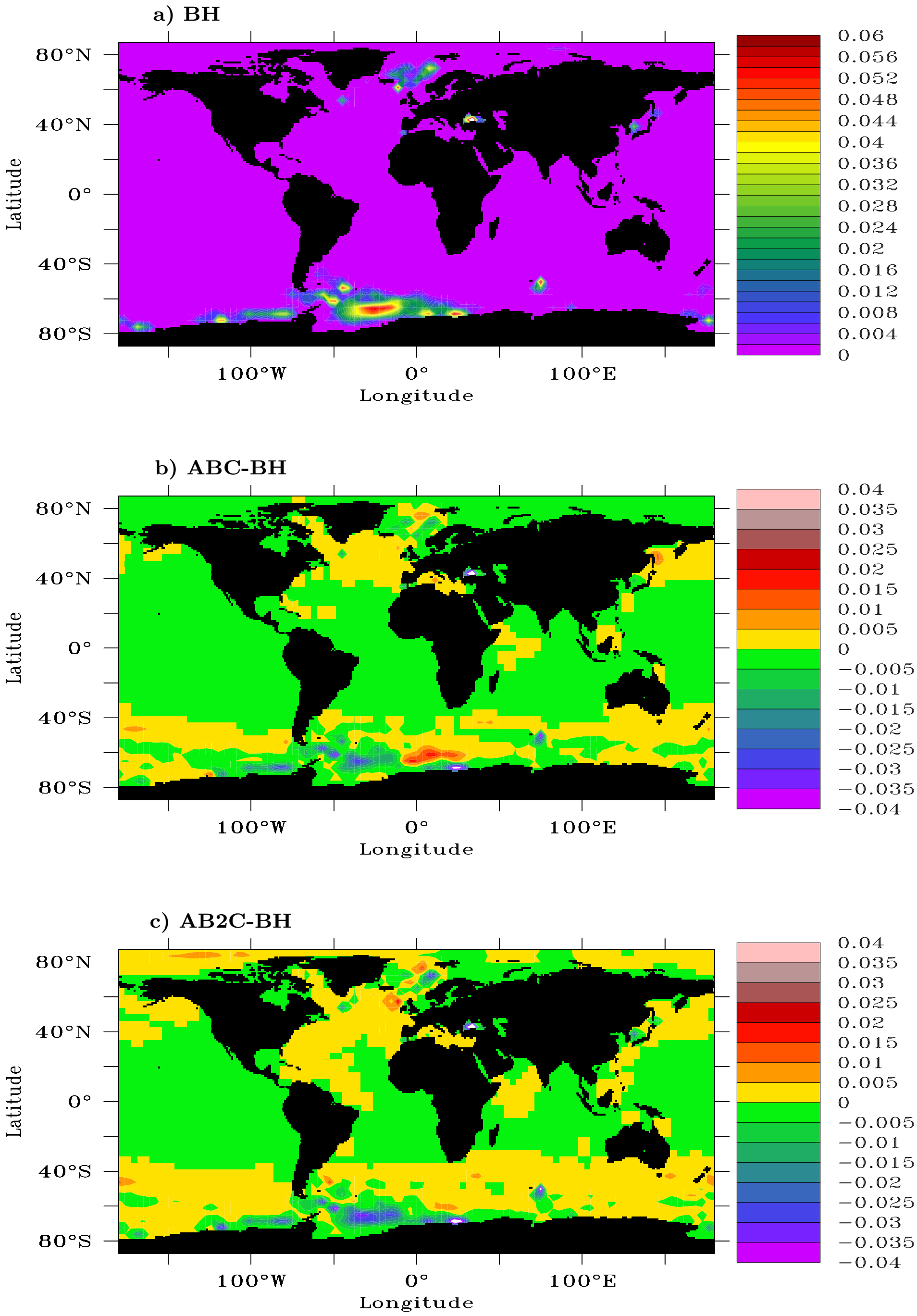

Figure 9: Same as Figure 8 but for K at 900 m.

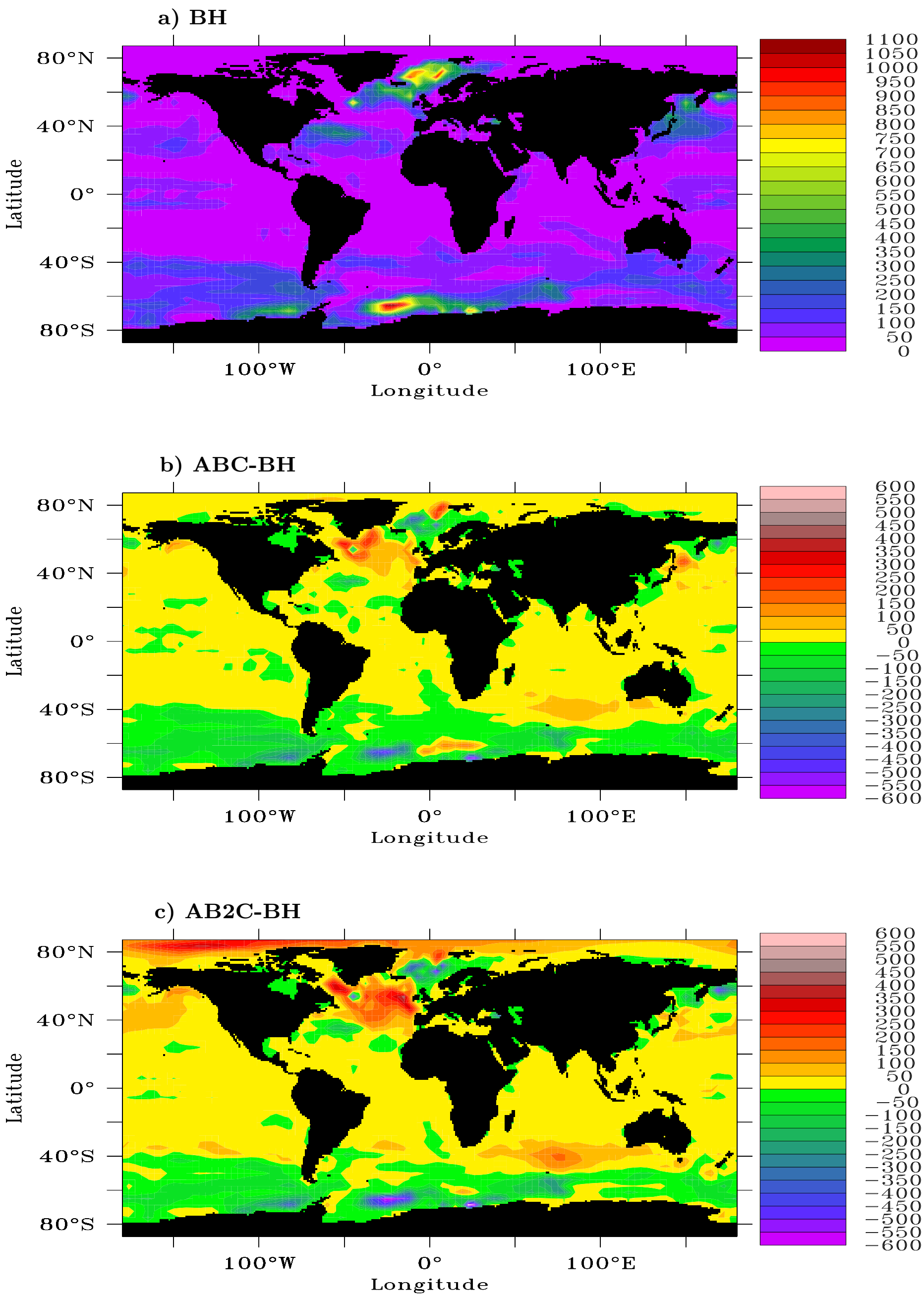

Figure 10: Horizontal distributions of mean convection depth in m for a) the time-mean in experiment BH and b) the difference between experiments ABC and BH and c) between experiments AB2C and BH.

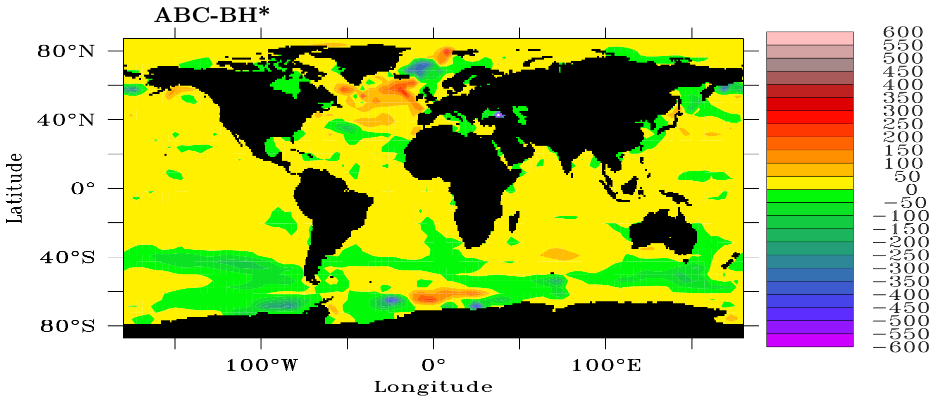

Figure 11: Horizontal distribution of the change in the mean convection depth in m between experiments ABC and BH*.

Table 1: Experiments done with MPI-OM and different versions of EMAD model. $\bar{\mathbf{x}}$ denotes the climatological fluxes and $\mathbf{x}^{'}$ the flux anomalies predicted by different versions of the EMAD model.

name	fluxes used	characteristics
BH	$\bar{\mathbf{x}} + \mathbf{x}^{'}$ $\mathbf{x}^{'}_t = \mathcal{B}\mathbf{y}^{'}_t, \quad (\mathbf{x}^{'} = H^{'}, \mathbf{y}^{'} = SST^{'})$	no fluctuations, with SST-feedback on heat flux
ABC	$\bar{\mathbf{x}} + \mathbf{x}^{'}$, $\mathbf{x}^{'}_t = \mathcal{A}\mathbf{x}^{'}_{t-1} + \mathcal{B}\mathbf{y}^{'}_t + \mathcal{C}\mathbf{n}_t$	with fluctuations + feedback
AB2C	$\bar{\mathbf{x}} + \mathbf{x}^{'}$, $\mathbf{x}^{'}_t = \mathcal{A}\mathbf{x}^{'}_{t-1} + \mathcal{B}\mathbf{y}^{'}_t + 2 \times \mathcal{C}\mathbf{n}_t$	with feedback + 2× fluctuations

Table 2: 200-year means of MOC-index and ACC-index in Sv in different experiments.

Experiment name	MOC-index	ACC-index
BH	17.1	200
ABC	18.3	148
AB2C	21.8	122
ECHAM5/MPI-OM	18.0	186